Microfluidic Systems with Ion-Selective Membranes

Zdenek Slouka, Satyajyoti Senapati, and Hsueh-Chia Chang

Department of Chemical and Biomolecular Engineering, University of Notre Dame, Indiana 46556; email: zslouka@nd.edu, ssenapat@nd.edu, hchang@nd.edu

Annu. Rev. Anal. Chem. 2014. 7:1.1–1.19

The *Annual Review of Analytical Chemistry* is online at anchem.annualreviews.org

This article's doi: 10.1146/annurev-anchem-071213-020155

Keywords

biosensing, depletion, electrokinetics, limiting current, molecular concentration

Abstract

When integrated into microfluidic chips, ion-selective nanoporous polymer and solid-state membranes can be used for on-chip pumping, pH actuation, analyte concentration, molecular separation, reactive mixing, and molecular sensing. They offer numerous functionalities and are hence superior to paper-based devices for point-of-care biochips, with only slightly more investment in fabrication and material costs required. In this review, we first discuss the fundamentals of several nonequilibrium ion current phenomena associated with ion-selective membranes, many of them revealed by studies with fabricated single nanochannels/nanopores. We then focus on how the plethora of phenomena has been applied for transport, separation, concentration, and detection of biomolecules on biochips.

1. INTRODUCTION

In recent years, the advancement of nanofabrication techniques has allowed the construction of nanostructures that are the workhorses of a new scientific discipline dealing with fluids confined in nanospaces—nanofluidics. They have catalyzed thorough investigations of electrokinetic phenomena in nanofluidic systems on the application of electric fields [alternative or direct current (DC)] and have revealed many unexpected and surprising phenomena. At this nanoscale confinement, surface charges and hydrodynamic slip phenomena at the channel walls often dictate the behavior of the whole system. The most important driving phenomenon is ion selectivity, when the transverse channel dimension is smaller than the Debye length, which can lead to large mobile ion concentration gradients, internal/external ion enrichment, extended polarized layers, surface electroconvection, water splitting, nonlinear ion current circuitry, current rectification, etc.

The concept of ion selectivity emerged long before nanofluidics, but nanofluidic research has greatly advanced our understanding of its effects. More than 70 years ago, ion-selective membranes started to be used in industrial water treatment processes such as electrodialysis and electrodeionization (1). These membranes are natural nanostructures because they contain nanopores decorated with surface charges. They are, however, much easier to synthesize and integrate into microfluidic systems than artificial nanostructures. In this review, we describe how knowledge garnered from artificial nanofluidic systems has led to new membrane-based microfluidic systems for the pumping, manipulation, preconcentration, and detection of biomolecules. Because they are inexpensive and can be easily integrated or inserted into a microfluidic chip, they are ideal for disposable point-of-care medical diagnostic biochips. They often offer better performance in limit of detection, sensitivity, selectivity, and target number than the cheaper paper-based devices and, unlike paper devices, can process large biomolecules such as chromosomal DNA.

Ion selectivity of such membranes also stipulates that the current is controlled by ion currents and not electron currents in electrodes or charge transfers by electrochemical reactions. As such, the membrane sensors are stable/reproducible and less sensitive to the presence of redox agents in the sample, and they do not require the fabrication of micro- or nanoelectrode sensors. Hence, membrane microfluidic devices are much more robust and inexpensive than electrochemical sensing devices.

2. CONCEPTS AND PHENOMENA

2.1. The Concept of Ion Selectivity

We offer only a cursory exposition of ion selectivity. It is currently an intensely researched topic, and interested readers are referred to several recent reviews (2–7). The concept of ion selectivity was formulated in the first half of the twentieth century and was later nicely described in a technical review by K. Sollner (8) in 1950. Sollner summarized the facts known about a material called collodion used to prepare porous membranes. He referred to those membranes as an electronegative membrane with preferential cation permeability, where the charge selectivity comes from acidic impurities present on the pores of the membrane. His technical review was based on a few previous papers by Meyer (9), Teorell (10, 11), and Donnan (12). Both Meyer and Teorell proposed the fixed charge theory of electrochemical membranes while Donnan worked out a theory of membrane equilibria. In the aforementioned review, Sollner (8, p. 141C) states the following:

> In the case of membranes of high and, in limiting cases, of ideal ionic selectivity—more correctly membranes which under a given set of circumstances are of ideal ionic selectivity—the picture becomes

> fairly simple. The pores are so narrow that the fixed charged wall groups prevent, by electric repulsion, the permeation of any ions of the same sign. The movement of the counter ions of the fixed charged groups alone is, therefore, the cause of all electrical effects observed with these membranes.

This statement essentially covers all the conditions that are required to observe ion selectivity. First, we need a fixed charge bound on a solid support and second, the space over the fixed charge has to be restricted to a distance at which the fixed charge has some effect. Although the first requirement is usually fulfilled by the dissociation of surface functional groups [or some other charging mechanism (13)] after soaking in a water solution, the second requirement can be estimated by evaluation of a so-called Debye length characterizing an electrical double layer that forms at the charged interfaces.

2.2. Electrical Double Layer

Due to the presence of some inherent functional groups on a solid surface, a fixed charge is established on the surface of the solid plate, rendering the plate either positively or negatively charged. The electrostatic interactions cause the free ions to rearrange by attracting the oppositely charged ions to the plate, creating an electrical double layer. The concentration of those oppositely charged ions (counterions) in this electrical double layer must be equal to the concentration of the fixed charge so that the system still obeys the electroneutrality condition. However, due to thermal fluctuation (diffusion in a continuum theory), the mobile counterions occupy a layer, the electric double layer, of finite thickness. The classical theory for electrical double layer can be found in standard texts (13, 14). The potential and concentration profiles of co- and counterions in the electrical double layer can be derived from the Poisson-Boltzman equation where a Debye screening length appears as a natural parameter. This Debye length is dependent on the ionic strength of the working buffer solution. Calculating the distance over which an excess of counterions over coions exists in the solution as a function of the electrolyte concentration reveals why nanospaces are necessary to provide ion selectivity. In nanospaces/nanochannels, the electrical double layers overlap, which makes them ion selective; e.g., counterions easily pass through, whereas coions are repelled. The Debye length is not the only factor important for ion selectivity. The concentration of the fixed charge is also an important parameter affecting ion selectivity (15, 16). Systems with low concentrations of the fixed charge exhibit only weak ion selectivity even though Debye layers overlap. In a recent review (17), a new quantity, volumic surface charge, was introduced. This quantity relates the surface charge density to the section height of a planar microchannel, which could be thought of as a measure of ion selectivity. In any case, it is clear that the concentration of the mobile ions and hence the ion current conductivity in the nanochannel are controlled by surface charge. As such, the channel ion conductivity is as much as 10 times higher than the bulk conductivity outside the channel, depending on the bulk ionic strength.

3. ION EXCHANGE MEMBRANES

3.1. Membrane Ion Current Circuits

Ion-exchange membranes are extensively used in many industrial applications, such as deionization or electrodialysis (1). There are many different types of ion-exchange membranes that can be classified according to their properties (18). Homogeneous ion exchange membranes (e.g., Nafion membranes) are made of coherent ion exchanger gel, whereas heterogeneous membranes contain ion-exchange particles embedded in an inert binder (**Figure 1*b***) (19). Most of these membranes

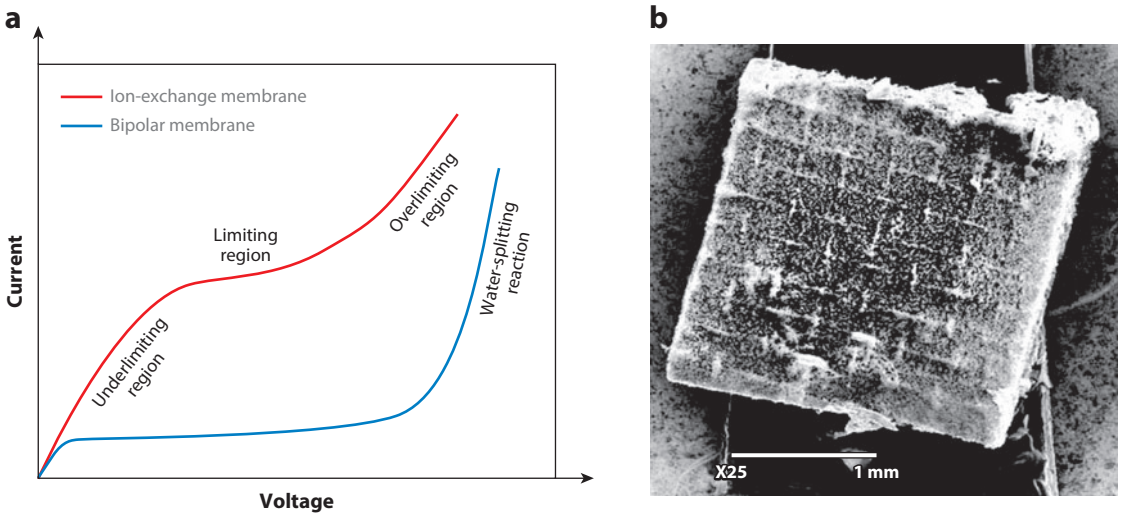

Figure 1

(*a*) Typical schematic representation of current voltage curves for an ion-exchange membrane (*red*) and bipolar membrane in the reverse bias (*blue*). (*b*) Scanning electron microscope image of a commercial heterogeneous polymeric membrane.

use sulfone anion ($R\text{-}SO_3^-$) for cation-exchange membranes and quaternary ammonium cation [$R\text{-}N^+(CH_3)_3$] for anion-exchange membranes as a fixed charge. Both groups are chemically very stable and capable of functioning properly over a large range of pH values. The charge borne by functional groups in nanochannels (SiO_2, Al_2O_3, COOH), however, can easily be neutralized in acid-base reactions, making the ion selectivity of nanochannels strongly pH dependent (20–22). The surface charge densities of ion-exchange membranes (23) and nanochannels (24) are usually on the order of mC/m^2. The pore size of those membranes prevents transport of molecules having molecular weights greater than 60–100 g/mol (25), a property that makes the membranes ion selective even for solutions with high ionic strength. For nanopores, however, the right solution with the proper ionic strength is absolutely necessary. Ion selectivity can be easily lost when solutions of high ionic strength are used (26–30). However, imparting the ion selectivity to the nanochannel by decreasing the ionic strength can be accompanied by a pH shift (31).

Although these ion-exchange membranes are mainly used in large-scale industrial processes for water treatment, they have also been integrated in microfluidic systems either to study fundamental electrokinetic processes (32–35) or to act as functional elements such as pH actuators (36) or biomolecule preconcentrators (37). One of the most interesting features of ion-exchange membranes is a nonlinear current voltage curve (CVC) (**Figure 1*a***) where two ohmic regions are connected through a limiting region, a behavior that was observed more than 60 years ago (38).

The origin of this nonlinearity is due to different transport numbers of mobile ionic species in the ion-selective membrane and surrounding electrolyte. At low voltages connected to the system, the electrical current is directly proportional to the voltage, which is referred to as the underlimiting region on the CVC. The ohmic resistance in this linear region can arise from the resistance outside the membrane or across the membrane, depending on the relative magnitude of each. However, with increasing voltage, the conductivity jump across the membrane begins to deplete bulk ions on one side of the membrane (depletion side) and enrich it on the other (**Figure 2*a***). The depletion layer near the membrane surface soon becomes the current controlling region of the system. At a certain critical voltage, the concentration of ions in the depletion region drops to almost

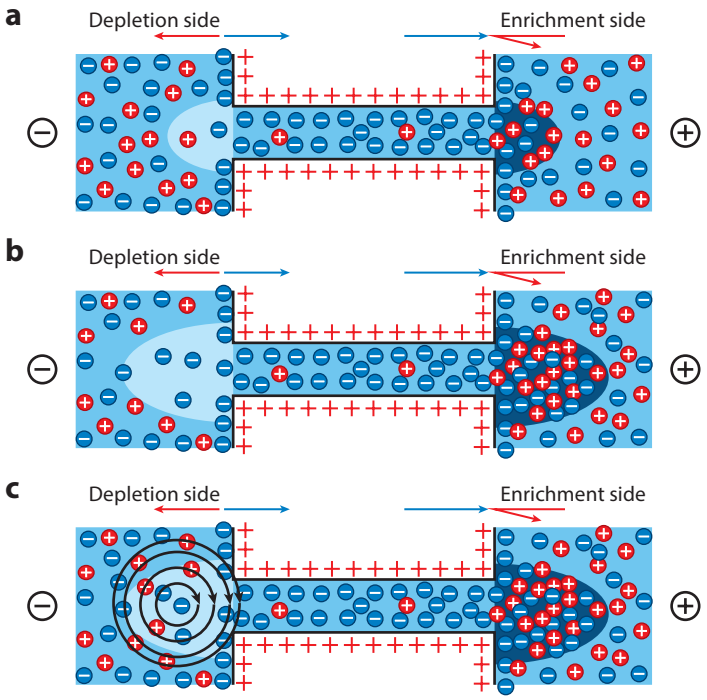

Figure 2

Schematics of the situation around an ion-exchange medium in an (*a*) underlimiting, (*b*) limiting, and (*c*) overlimiting region.

zero, and the current starts to saturate (**Figure 2*b***). This region on the CVC appears as a limiting region. This behavior was described by the concentration polarization theory (39). However, experimental data showed that with increasing voltage an inflection occurs on that curve, giving rise to a second linear region called the overlimiting region. This overlimiting region is a mystery and has been attributed to many possible effects: (*a*) electroconvection, (*b*) water splitting, (*c*) the exaltation, (*d*) natural convection, or (*e*) changes in ion selectivity (40–44). All these effects can contribute to the overlimiting current depending on the experimental setup. However, electroconvection in the depletion region is considered the main mechanism of the overlimiting current (**Figure 2*c***), as it was recently captured in real-time fluorescent experiments with both ion-selective nanochannels (28) and membranes (33, 35). Placing an agar gel in the depletion region is known to suppress the overlimiting current (45), which is also consistent with the electroconvection mechanism.

This electroconvection explained by Rubinstein et al.'s (43) microvortex instability essentially destroys the depletion region by mixing it with the electrolyte bulk. Vortices occurring on the depletion side of the membrane were confirmed using both theoretical analysis (46, 47) of the system and numerical solution of full Navier-Stokes/Poisson-Nernst-Planck models (15, 48–50). Similar CVC with three regions associated with underlimiting, limiting, and overlimiting currents have also been reported for a single nanopore (22, 29, 51). The overlimiting region was caused by Rubinstein's electroconvection instability, which arrested the growth of the depletion region (28). Yossifon & Chang (52) even observed two limiting regions when charged particles were added to the system and created a second ion-selective layer. This gave rise to the second overlimiting region. It was further shown that the pore geometry and the depth of the connecting chamber can have a profound effect on CVC (51). Yossifon et al. (53) showed that changing the width of

a nanochannel (from 2.5 mm down to 50 μm) can lead to the loss of the limiting region on the CVC, even though a pair of vortices caused by induced charged electroosmosis was still observed at the entrance to the nanochannel. Such a linear CVC is often reported for small symmetrical nanochannels as well (21, 54), unless a fixed charge at the entrance to the nanopore has opposite sign to that inside the nanopore (54), which leads to saturation of the current. The generation of depletion and enrichment regions around nanopores has frequently been observed and used for preconcentration of large molecules (55). A quantitative model (56) and full numerical models (57) of a single nanopore connected to microchambers have confirmed concentration polarization and formation of depletion and enrichment regions around the nanopores. Interestingly, no vortices were observed in systems where a nanochannel with developed ion concentration polarization was used for preconcentration. Systems in which a small piece of a Nafion membrane was used instead, however, revealed vortices in the depletion region (37, 58).

Interestingly, ion-permselective particles (59, 60) were also shown to exhibit depletion and enrichment behavior accompanied with obscure and complex electrokinetic vortices (60). The origin of these microvortices is different from those predicted by Rubinstein's instability theory, as was summarized in a review by Chang et al. (61).

3.2. Bipolar Membranes

By stacking cation- and anion-exchange membranes, we create a so-called bipolar membrane. Bipolar membranes behave as ion-diodes with a strong rectification effect—the ion current is very different for forward and reverse biases. The forward bias causes the formation of an ion-enriched region at the bipolar junction and exhibits a linear CVC ohmic curve (**Figure 3*a***). With reverse bias, the ions are depleted from the bipolar junction, and the local electric field increases with decreasing ionic strength (**Figure 3*b***). At a sufficiently high voltage, the electric field at the bipolar junction becomes sufficiently high to split water, and the junction becomes an ionic reactor that continuously generates H+ and OH− ions (36, 62–65). The resulting water-splitting current produces an overlimiting current that is higher than any other mechanism, including that due to electroconvection by the microvortex instability.

3.3. Electroosmotic Flow Across Membranes and Backpressure

There have been very few studies on the importance of electroosmotic (EO) flow to ion flux across ion-selective membranes, but it is generally agreed that it is significant for membranes with larger pores (>10 nm). However, the pumping action of nanoporous membranes, particularly solid state silica membranes in capillaries, has been well studied in the past decade (66). EO flow through a nanoporous membrane is fed into an open microfluidic channel. To ensure flow balance, a large backpressure builds up at the membrane/channel interface such that a pressure-driven flow can be driven downstream along with a pressure-driven backflow in the membrane to reduce the EO flow. Such EO pumping is ideal for driving flow in a biochip, as it involves no moving parts and can be driven by miniature power sources. However, it is extremely inefficient and was thought to be insufficient to overcome the large hydrodynamic resistance of microchannels on a chip. Paul et al. (67) first realized that this shortcoming of EO flow can be eliminated if a nanoporous ion-selective membrane is inserted into the microfluidic channel as a pumping section. The inefficiency of EO flow is caused by the electroneutral bulk being driven by an electric body force confined to the nanoscale space charge region within one Debye length λ of the charged surface, where it is balanced by a large hydrodynamic shear. With a nanopore smaller than the Debye length, this unfavorable force budget would be eliminated. However, a nanopore much

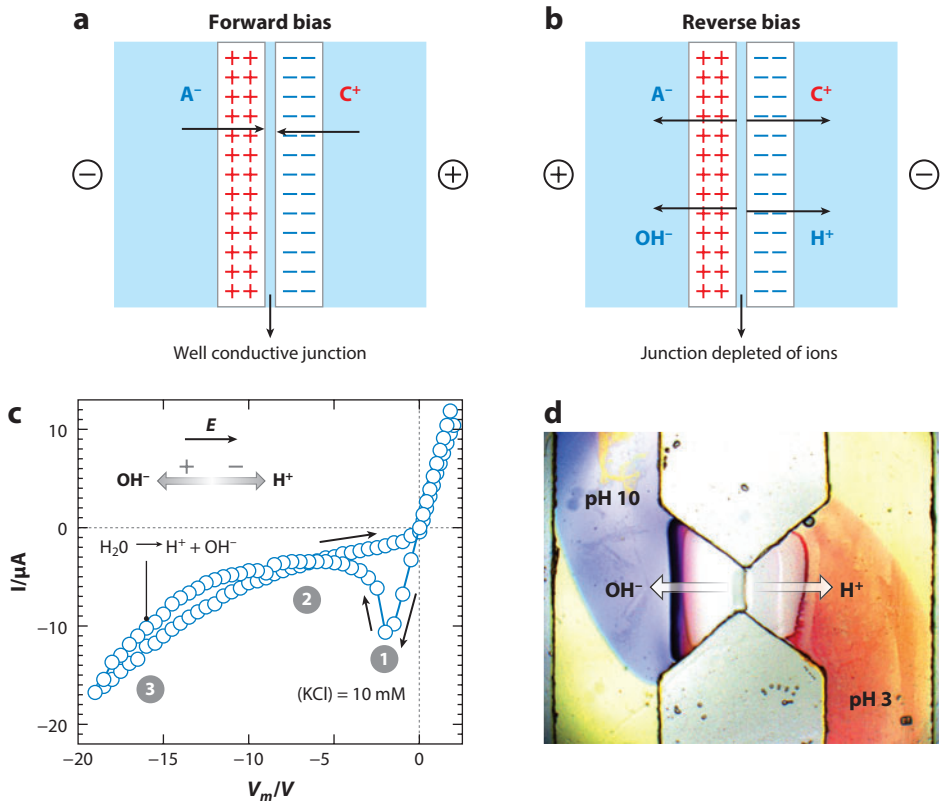

Figure 3

Schematic representation of a bipolar membrane connected in the (*a*) forward and (*b*) reverse bias. "+" and "−" signs represent the surface charge of the membranes. (*c*) I-V curve measured by Cheng & Chang (36) in the reverse bias region showing large overlimiting current and hysteresis. The spike at −2V during the backward scan is due to residual ions from water splitting in the bipolar membrane. Equilibration to the limiting current at −5V occurs after the depletion of residual ions. The numbers 1, 2, and 3 represent the hysteresis, saturation, and water-splitting regimes, respectively. (*d*) Image of pH-sensitive dye across the bipolar membrane showing ejection of H^+ and OH^- ions.

smaller than the Debye length would then produce excessive hydrodynamic stress, higher than even that within a Debye layer in a larger channel. Hence, an optimum EO pump would have a pore size that is roughly the same as λ of the medium—a weakly ion-selective medium. To ensure continuous flow into a downstream microchannel, a pressure maximum would then develop at the end of the nanoporous EO pump region, such that a backpressure reduces the high EO flow in the nanoporous pump and drives a pure pressure-driven flow in the microchannel. In the past 15 years, such nanoporous EO pumps have been developed by packing nanoparticles, fabricating polymer frits or nanoporous alumina in a chip, and sol-gel chemistry synthesis with an on-chip pressure as high as a few atmospheres for the most mechanically strong pumps (68–72). In **Figure 4*a***, we show the scanning electron microscope (SEM) image of a nanoporous silica monolith that has been synthesized by sol-gel chemistry in a silica microcapillary and the large pressure (2 atm) it can sustain at the end of the monolith (**Figure 4*b***). Such large backpressures can drive flow downstream in open channels or even sustain robust electrosprays at the end of the chip such that the electric field both supplies on-chip EO pumping and generates the electrospray (73).

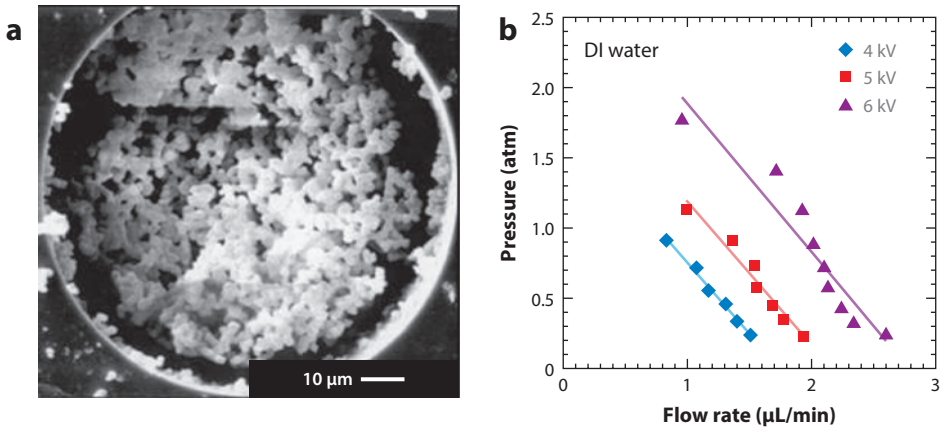

Figure 4

(*a*) Scanning electron microscope image of a nanoporous silica membrane in a glass capillary. Image by Wang et al. (71). (*b*) The no-load pump curve measured by compressing an air bubble at the end of a closed capillary shows a maximum pressure of several atmospheres. Abbreviation: DI, distilled.

3.4. Mixing By Nanoporous Granules

Ion depletion/enrichment across the membrane and vortices in the depleted region that are shown in **Figure 2** for a flat membrane or nanoslot can also be seen across a spherical ion-exchange granule (**Figure 5**). However, the mechanism for the vortices is not due to the Rubinstein instability but to a Dukhin mechanism because of a tangential field around the granule (60). These vortices can be used to enhance the assay time of many transport-limited biological reactions (74).

3.5. Sensitivity to Surface Molecules and Membrane Biosensors

Both the depletion region responsible for the limiting current and the microvortices responsible for the overlimiting current in **Figure 2** are very close to the membrane surface. In fact, the extended polarized region responsible for the microvortex Rubinstein instability is only slightly larger than the Debye length λ, at roughly 100 nm. Hence, the presence of large biomolecules such as DNA can suppress the microvortices and reduce the overlimiting current. This suppression should be even more pronounced if the DNA is of opposite charge from the membrane, such that the depletion and extended space charge regions cannot fully develop. However, at high coverage by an oppositely charged surface molecule, a monolayer may develop, and a bipolar membrane can form. The water-splitting mechanism of **Figure 3** would then reverse the trend and significantly enhance the overlimiting current. This inversion in the overlimiting current suppression was indeed found in a recent report by Slouka et al. (33). As seen in **Figure 6**, negatively charged ssDNAs physisorbed onto positively charged anion-exchange membranes produce two different shifts in the overlimiting current—reducing it at low concentrations but enhancing it at high concentrations. Evidence of water splitting was also seen in the latter case by using pH-sensitive dye. This experiment immediately suggests the possibility of biosensing, if probes can be functionalized onto the depletion side of the membrane. Such a membrane sensor technology would work at the high voltage overlimiting current region but not at the mV region typical for electrochemical sensing techniques. Moreover, this works because ion currents are involved and hence the sensors are not sensitive to redox agents in the sample.

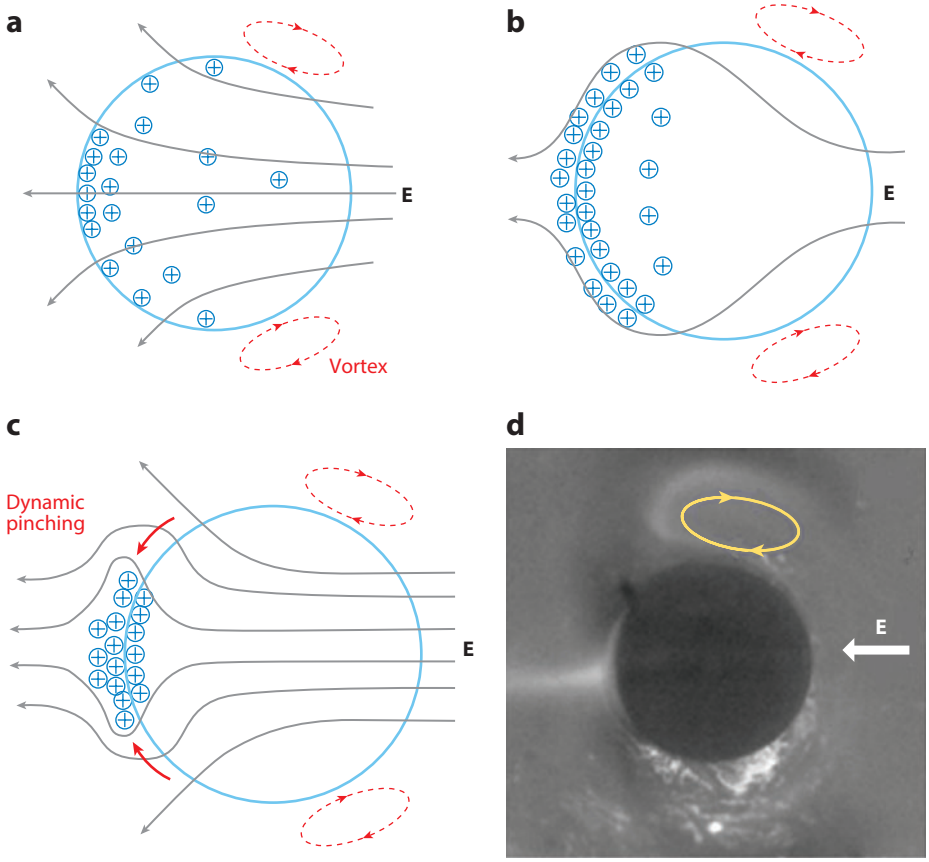

Figure 5

Ion enrichment at one pole of an ion-exchange granule and vortex pair generation at the other pole when an electric field is applied across an ion-selective granule. (74). (*a*) Convective charging of the granule by asymmetric vortices at the right. (*b*) Saturation of the double layer by counterions exiting the granule and field screening. (*c*) Dynamic double-layer pinching toward the ejection pole. (*d*) A real image showing the polar ejection and the asymmetric vortices on the other hemisphere.

3.6. Rectification in Nanopores

A phenomenon associated with ion selectivity of nanochannels, which has not been observed for ion-exchange membranes, is rectification observed for nanochannels with a certain type of asymmetry (75, 76). This asymmetry can be caused by the geometry of the nanopores [e.g., a conical shape (21) or a nanopore connected to asymmetric chambers (77, 78)], concentration (79), and pH (80) gradient imposed on the nanochannel or a sudden change in surface charge (24). These asymmetries cause the ion selectivity to vary along the nanochannel in two ways: either (*a*) from strong to weak ion selectivity to the same type of ions (nanochannels with an asymmetry in geometry or with a concentration gradient) or (*b*) two regions of the nanochannel have ion selectivity to cations and anions (nanochannels with a pH gradient or with a change in polarity of the surface charge), respectively.

In conical nanopores, the diameter of the pore increases, thus rendering the tip ion selective, whereas the larger opening does not possess that strong ion selectivity (81). The cause for

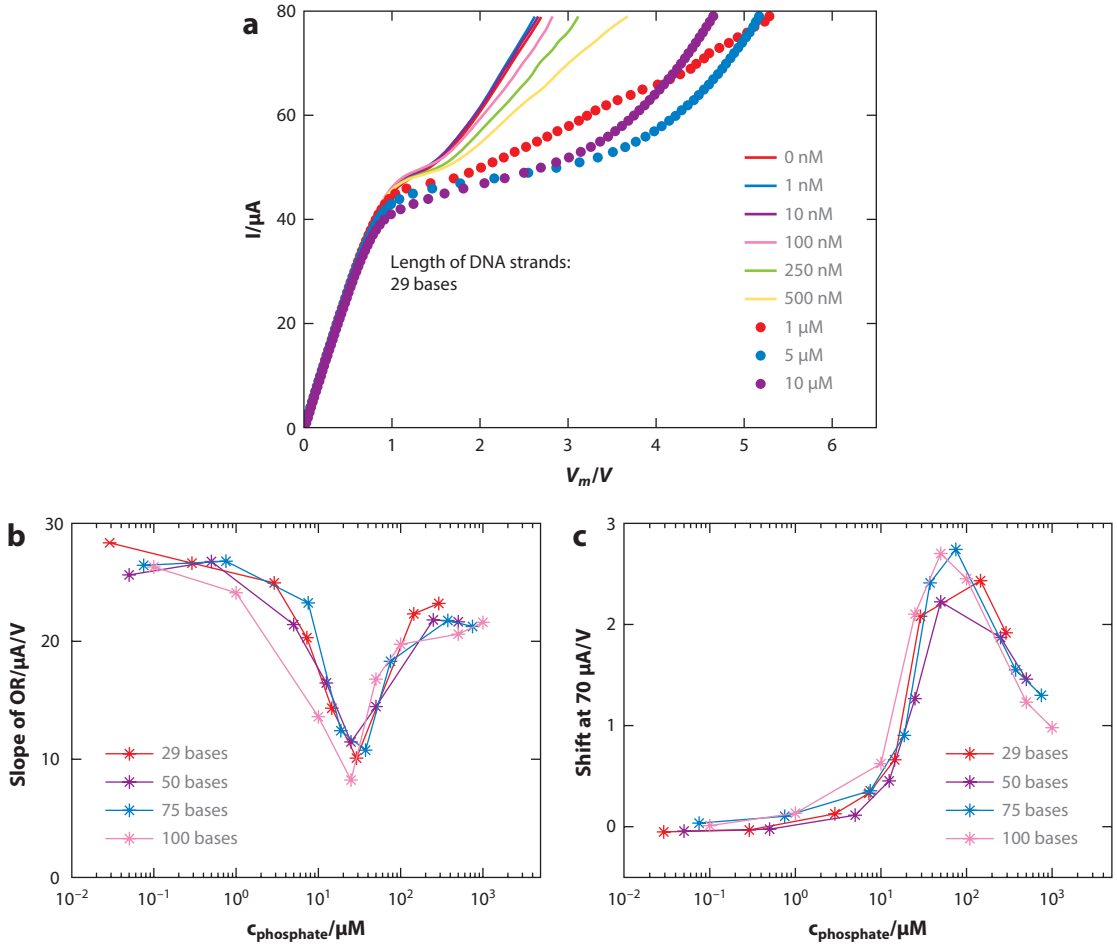

Figure 6

Current voltage curve of an anion-exchange membrane with physisorbed ssDNA (29 nucleotides long) present at different concentrations. (*a*) A reduction in the overlimiting current occurs below 1 μM, but an upward shift develops beyond this critical target concentration. (*b*) Slope of the OR. (*c*) Shift at 70 μA plotted against the concentration of the phosphate groups bound on each DNA sample. Abbreviation: OR, overlimiting region.

rectification in these channels is not yet fully understood (21), but formation of enrichment and depletion regions in the body of the conical nanopore can explain this behavior. The formation of enrichment and depletion regions in the conical nanopore was confirmed by simulations (82) as well as experiments with a fluorescent dye (83). However, the effect of the surface charge concentration relative to the bulk ionic strength can be very important for conical nanopores (16) and can lead to a curious rectification inversion phenomenon across a critical concentration. Bipolar nanopores with a change in the surface charge (positive and negative) present a group of nanopores similar to bipolar membranes (84, 85). These systems reach the highest rectification factor, and the explanation of this behavior is straightforward. Although a high conductivity region develops in the nanochannel for a forward bias, a low conductivity region is responsible for low currents in the reverse bias connection (86, 87). Interestingly, Cheng & Guo (24) observed a breakdown

of the bipolar nanofluidic diode, which was attributed to a water-splitting reaction occurring at the interface between negatively charged silica and positively charged alumina. The rectification curve was also observed for biological nanopores with imposed pH gradient (80) or engineered nanopores that possess spatially separate regions of opposite charge (88). Cheng & Guo (79) studied the effect of concentration gradient imposed on homogeneous silica nanochannels. The concentration gradient causes the nanochannel to have different Debye lengths at both ends, which is then responsible for rectification. Although for the forward bias the depletion develops at the low concentration side of the nanochannel and the nanochannel loses its ion selectivity, the reverse bias depletes the ions on the high concentration side of the nanochannel, which enhances the ion selectivity of the nanochannel. These effects result in the formation of high conductive and low conductive solutions in the nanochannel. It is possible that such rectification mechanisms of nanochannels can produce new membrane biosensors, if they are transferred to membranes; the asymmetric charge distribution is the most promising one. They could also be used to improve single pore stochastic sensing (89–92).

4. APPLICATIONS

We review several microfluidic technologies that have been developed based on the phenomena described in the previous sections, culminating in an integrated chip that combines several of such technologies. These components pump the sample through the chip (see **Figure 4**), concentrate analytes at certain sensors, mix the reactants, and detect specific molecular targets. Because they are all based on ion currents, it is unnecessary to have microelectrodes within the chip. All electrical connections can be inserted through easily fabricated salt bridges through orifices that also allow fluid exchange.

4.1. Analyte Concentration

The ion depletion at the limiting current region can span across the entire microchannel and be used to prevent convection of charged molecules into the depletion zone, thus trapping them at the upstream edge of the depleted region. Han's group has fabricated nanochannels and proton-hopping Nafion membranes to allow effective concentration of analytes (55, 93, 94). Ion-selective membranes allow easier fabrication of such on-chip analyte concentration modules. As shown in **Figure 7*a***, a cation-exchange membrane UV-polymerized in a microslot bridging two microfluidic channels can induce deionization under voltage biases. The ion-depletion region functioning as an energy barrier traps the molecule passing across it in an electroosmotic flow tangential to the membrane on the side. The UV-curable ion-selective membrane offers superior concentration efficiency and processability to that of prior works using microfabricated nanochannels or Nafion resins. Unlike the 100-nm-thick nanochannels and surface-patterned Nafion thin films, the proposed membrane slot has the same depth as the microfluidic channel, yielding a large junction area. The large cross-sectional area provides greater ion current and better control of ion depletion in the microchannels. Therefore, preconcentration can be achieved in a few seconds. The fluorescence image in **Figure 7*b*** shows the concentration of labeled molecules by two to three orders of magnitude in 10 s from a solution being pumped by electroosmosis from the left to right in the top microfluidic channel, after 10 V is applied across the membrane. Moreover, the UV-curable ion-selective membrane adheres well to glass surfaces functionalized with acrylate-terminated silane, whereas Nafion has poor adhesion to most solid surfaces and the process is more operator dependent.

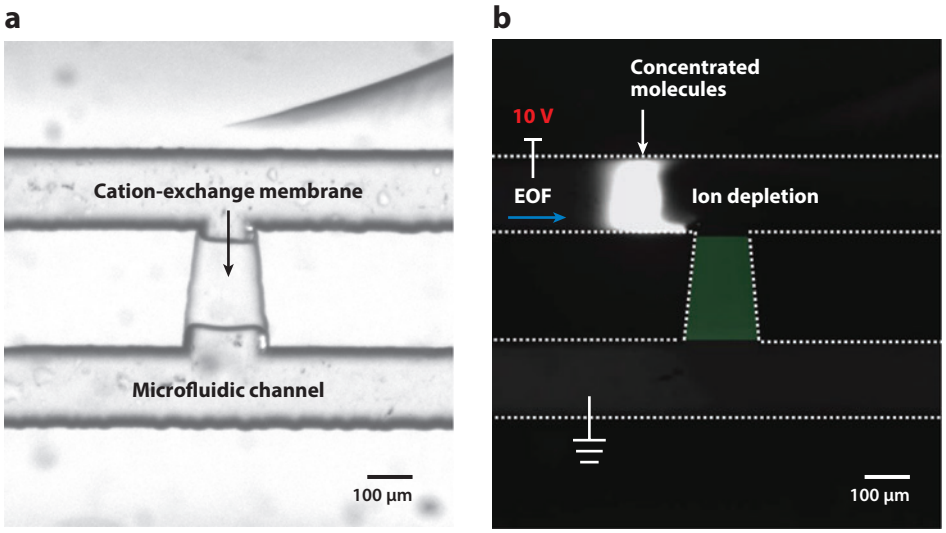

Figure 7

(*a*) A UV cured cation-exchange membrane embedded in a microfluidic channel. (*b*) The membrane produces a depletion region to concentrate charged dye molecules by two to three orders of magnitude in a flowing stream. The scale bars in the images indicate 100 µm. Abbreviation: EOF, electro-osmotic flow.

4.2. Integrated Membrane Point-of Care Diagnostic Unit

Ion concentration polarization on ion-exchange membranes can be employed for separation, concentration, and detection of biomolecules similarly to ion-selective channels. One of the main challenges that researchers often encounter is device fabrication with ion-exchange membranes. These membranes are generally incompatible with the materials traditionally used for fabrication of microfluidic systems. One of the major reasons is the swelling of the membranes when exposed to water solutions. The increase in volume after swelling of the membranes is approximately 50%, and the swelling forces are enormous (like charge repulsion of the fixed functional groups). However, the proper functioning of these membranes requires tight sealing within a microfluidic system so that no current can bypass the membrane. We solved this challenge by using molding resins that allow the tight embedding of these membranes in some functional elements that can be later integrated on a microfluidic chip.

Because ion-exchange membranes develop depletion and enrichment regions when a DC electrical field is applied, we used these effects and a novel nucleic acid sensing mechanism to construct an integrated point-of-care diagnostic platform that integrates three functionally independent units, as illustrated in **Figure 8*a***. The chips are fabricated through thermal bonding of polycarbonate sheets that have been cut to form internal microchannels and orifices for the insertion of the electrode salt bridges, flow tubing, and sample filters. This three dimensional architecture with vertical integration allows precise control of all the membrane ion circuits on the chip by an external electronic instrumentation, with the ion currents as sensing variables as well as control variables.

The first unit is a pretreatment unit that allows extraction of negatively charged biomolecules (DNA and RNA mainly) from cell lysates through a thin layer of agar gel (**Figure 9*a***), whose working principle is similar to gel electrophoresis. The negatively charged nucleic acid molecules accumulate on the enrichment side of a cation-exchange membrane, which prevents the negatively

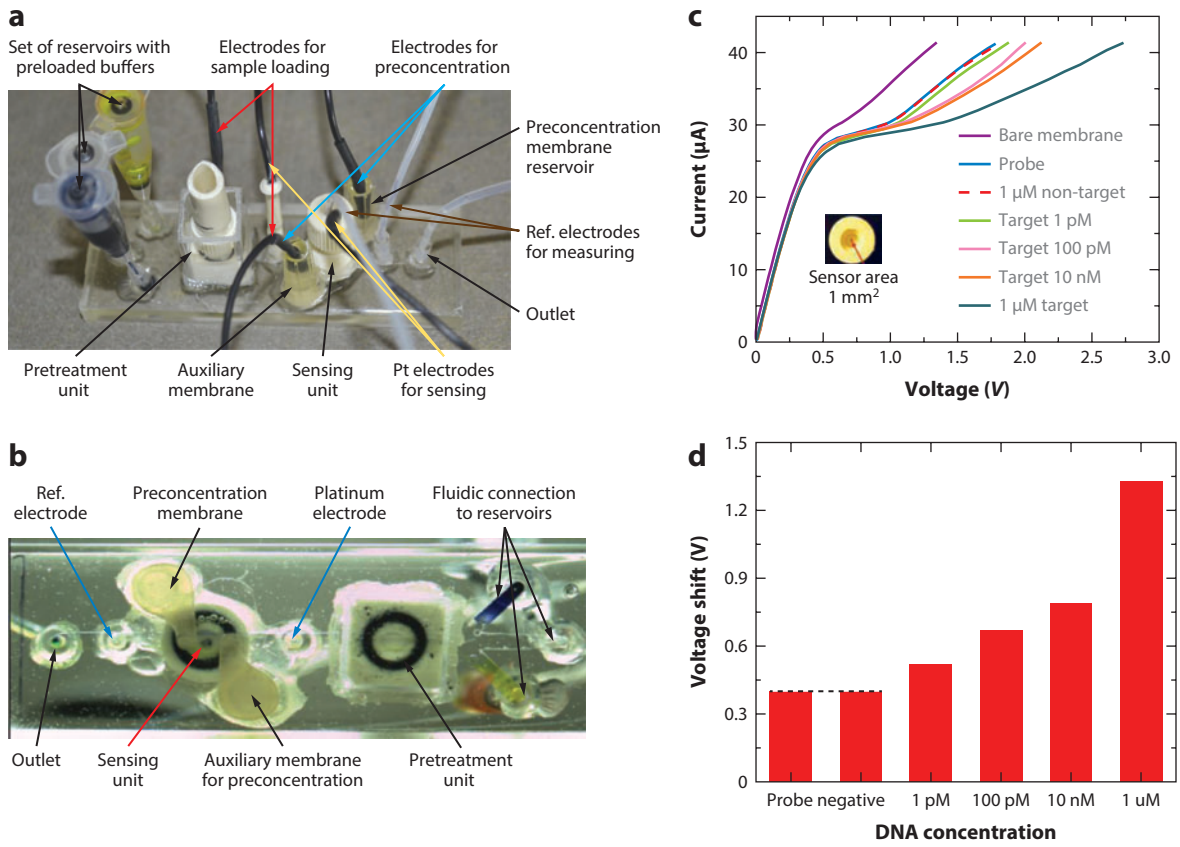

Figure 8

(*a*) Top and (*b*) bottom view of an ion-exchange-membrane-based integrated point-of-care diagnostic platform. pM to μM concentrations of target DNA is added to the same sensor to evaluate the dynamic range. (*c*) Results show an improvement in the sensor sensitivity down to 1 pM concentration by reducing the sensor area to 1 mm^2 (*inset*). (*d*) Histogram showing changes in potential (from bare membrane) at different DNA concentrations.

charged molecules to leave the main channel by both electrostatic repulsion and the sieving effect. When those negatively charged molecules are loaded into the main channel, another unit called the preconcentration unit collects and concentrates all the loaded molecules at a specific location in the main channel (**Figure 9*b***). The preconcentration unit consists of two cation-exchange membranes. One membrane creates a depletion region within the main channel that functions as an ionic filter and the other is just an auxiliary membrane that allows us to connect the electrical field to a specific part of the main channel. The position of the preconcentration slug can be controlled by counterbalancing the convective flow and depletion driven by the voltage applied on the system.

This feature which decouples the control of the flow rate and the extension of depletion makes our platform unique. By positioning the preconcentration slug right at a detection unit, we can achieve very fast detection of target nucleic acids. The detection unit is based on a charge inversion phenomenon that occurs when negatively charged nucleic acid molecules adsorb on a positively charged anion-exchange membrane. The charge inversion brings about two main effects: (*a*) It suppresses vortices on the membrane and (*b*) it enhances a water-splitting reaction at an interface

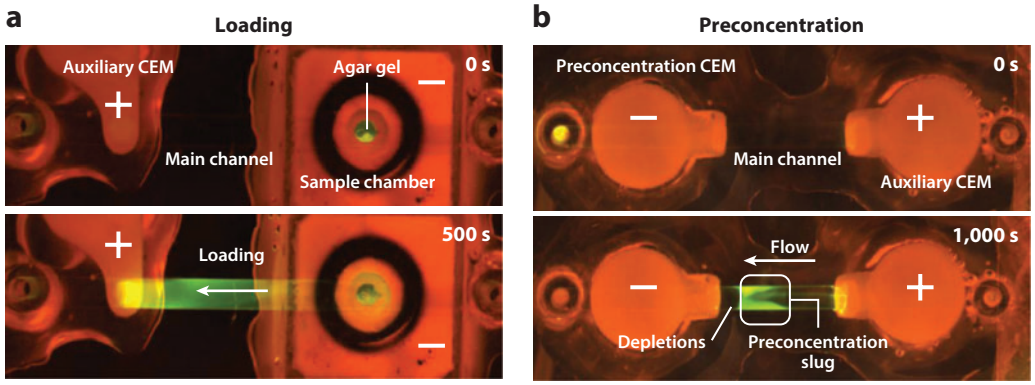

Figure 9

(*a*) Loading of fluorescently labeled DNA from a sample chamber and accumulation of the DNA on the enrichment side of the CEM. (*b*) Preconcentration of fluorescently labeled DNA. Abbreviation: CEM, cation-exchange membrane.

between the positive membrane and negatively charged molecules that behaves as a bipolar junction. In turn, this behavior is reflected in the CVC, where the limiting region prolongs, and the overlimiting region shifts toward higher voltages. This shift in the overlimiting region of the CVC indicates the presence of negatively charged molecules on a membrane surface. When such a membrane is first functionalized with a target-specific short oligoprobe, it makes the sensor specific to that target pathogen. Any shift in the CVC will indicate the successful capture of target nucleic acid by increasing the net negative charge on the membrane surface with a hybridization event. An example of a nucleic acid detection signal is plotted in **Figure 8*c*,** which shows pM to μM

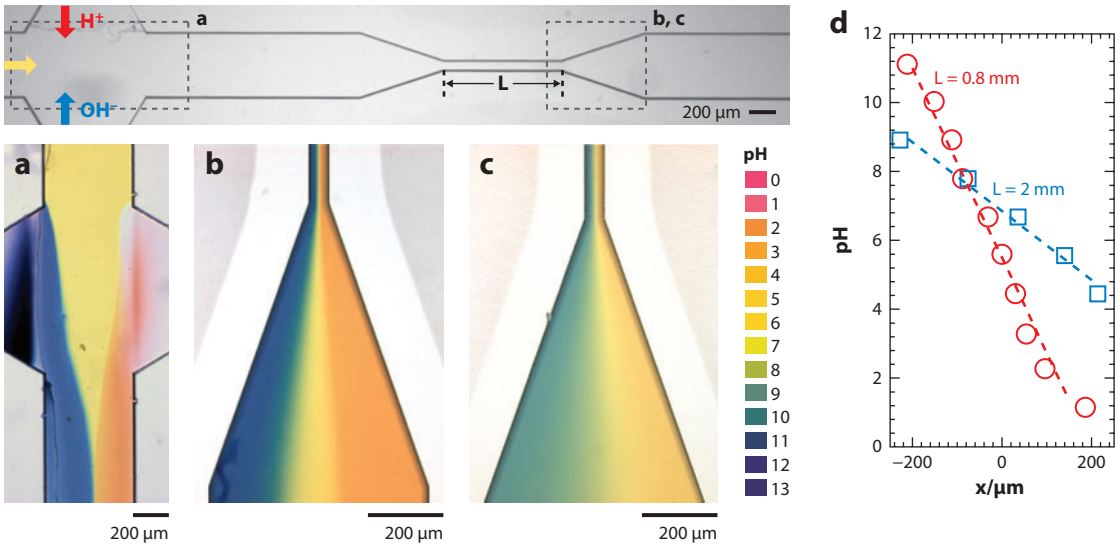

Figure 10

(*a*) Abrupt pH profile builds up near the pH actuators upstream. Different pH gradients were generated across a 500-μm-wide channel downstream after passing through a (*b*) 0.8-mm-long or (*c*) 2-mm-long, 50-μm-wide narrowed channel. (*d*) pH profiles across the downstream of channel in panels *b* and *c*.

dynamic range detection of DNA molecules on a 1-mm^2 sensing area. The simple fabrication and low cost make this detection platform very useful in point-of-care diagnostics.

4.3. Membrane Molecular Separation Techniques

We have also developed a pH actuation unit based on the water-splitting reaction occurring in the bipolar junction by a pair of ion exchange membranes when reverse bias is connected to the system (36). By using two bipolar junctions integrated into a single microchannel, we created a system where the production of H^+ and OH^- ions is controlled independently by applying different voltages on the junction. Mixing these two ions generated at the bipolar junctions downstream the main channel creates either a gradient in pH across the channel or a solution of a given pH (**Figure 10*a***). This technology thus provides an easy pH tuning tool in a microfluidic channel that can be employed, e.g., for isoelectric focusing separation of proteins (**Figure 10*b***).

5. CONCLUSION

Ion-selective membranes offer several unique functionalities for microfluidic systems that cannot be easily introduced by mechanical, electrochemical, and other techniques in microfluidics. They allow on-chip pumping, mixing, pH actuation, analyte concentration/separation, and target sensing—just about all the functionalities one needs for point-of-care diagnostics or even mass spectrometry interfaces. Moreover, they can be integrated into biochips with minimal effort, thus allowing disposable biochips, and can be easily controlled with a supervising electronic instrument detached from the disposable biochips. The biochips also lend themselves to easy rapid prototyping so that different designs can be optimized and tested. We see membrane microfluidics as a promising direction for field-used portable diagnostic devices.

DISCLOSURE STATEMENT

The authors are not aware of any affiliations, memberships, funding, or financial holdings that might be perceived as affecting the objectivity of this review.

ACKNOWLEDGMENTS

This work is supported by Army Corps of Engineers W9132T, Walther Cancer Fund 0120, USDA 2012-67005-19589, and NSF-CBET 1065652.

LITERATURE CITED

1. Strathmann H, Grabowski A, Eigenberger G. 2013. Ion-exchange membranes in the chemical process industry. *Ind. Eng. Chem. Res.* 52:10364–79
2. Park S, Chung T, Kim H. 2009. Ion bridges in microfluidic systems. *Microfluid Nanofluid* 6:315–31
3. Mortensen NA, Olesen LH, Okkels F, Bruus H. 2007. Mass and charge transport in micro and nanofluidic channels. *Nanoscale Microscale Thermophys. Eng.* 11:57–69
4. Yuan Z, Garcia AL, Lopez GP, Petsev DN. 2007. Electrokinetic transport and separations in fluidic nanochannels. *Electrophoresis* 28:595–610
5. Sparreboom W, van den Berg A, Eijkel JCT. 2010. Transport in nanofluidic systems: a review of theory and applications. *New J. Phys.* 12:015004
6. Piruska A, Gong M, Sweedler JV, Bohn PW. 2010. Nanofluidics in chemical analysis. *Chem. Soc. Rev.* 39:1060–72

7. Napoli M, Eijkel JCT, Pennathur S. 2010. Nanofluidic technology for biomolecule applications: a critical review. *Lab Chip* 10:957–85
8. Sollner K. 1950. Recent advances in the electrochemistry of membranes of high ionic selectivity. *J. Electrochem. Soc.* 97:C139–51
9. Meyer KH. 1937. Artificial membranes: their structure and permeability. *Trans. Faraday Soc.* 33:1073–80
10. Teorell T. 1935. Studies on the "diffusion effect" upon ionic distribution I. Some theoretical considerations. *Proc. Natl. Acad. Sci. USA* 21:152–61
11. Teorell T. 1935. An attempt to formulate a quantitative theory of membrane permeability. *Proc. Soc. Exp. Biol. Med.* 33:282–85
12. Donnan FG. 1911. Theory of the balances of membranes and potential of membranes at the existence of non dialysing electrolytes—a contribution to physical chemical physiology. *Z. Elektrochem. Angew. Phys. Chem.* 17:572–81
13. Chang HC, Yeo LY. 2010. *Electrokinetically Driven Microfluidics and Nanofluidics*. Cambridge/New York: Cambridge Univ. Press.
14. Daiguji H. 2010. Ion transport in nanofluidic channels. *Chem. Soc. Rev.* 39:901–11
15. Postler T, Slouka Z, Svoboda M, Pribyl M, Snita D. 2008. Parametrical studies of electroosmotic transport characteristics in submicrometer channels. *J. Colloid Interface Sci.* 320:321–32
16. Yan Y, Wang L, Xue JM, Chang HC. 2013. Ion current rectification inversion in conic nanopores: nonequilibrium ion transport biased by ion selectivity and spatial asymmetry. *J. Chem. Phys.* 138:044706
17. Plecis A, Pallandre A, Haghiri-Gosnet AM. 2011. Ionic and mass transport in micro-nanofluidic devices: a matter of volumic surface charge. *Lab Chip* 11:795–804
18. Tanaka Y. 2007. Chapter 1: Preparation of ion exchange membranes. In *Membrane Science and Technology*, ed. T Yoshinobu, pp. 3–16. Amsterdam: Elsevier
19. Prakash P, Hoskins D, SenGupta AK. 2004. Application of homogeneous and heterogeneous cation-exchange membranes in coagulant recovery from water treatment plant residuals using Donnan membrane process. *J. Membr. Sci.* 237:131–44
20. Fornasiero F, Bin In J, Kim S, Park HG, Wang Y, et al. 2010. pH-Tunable ion selectivity in carbon nanotube pores. *Langmuir* 26:14848–53
21. Siwy ZS. 2006. Ion-current rectification in nanopores and nanotubes with broken symmetry. *Adv. Funct. Mater.* 16:735–46
22. Chang CC, Yeh CP, Yang RJ. 2012. Ion concentration polarization near microchannel-nanochannel interfaces: effect of pH value. *Electrophoresis* 33:758–64
23. Kang MS, Choi YJ, Moon SH. 2004. Effects of charge density on water splitting at cation-exchange membrane surface in the over-limiting current region. *Korean J. Chem. Eng.* 21:221–29
24. Cheng LJ, Guo LJ. 2009. Ionic current rectification, breakdown, and switching in heterogeneous oxide nanofluidic devices. *ACS Nano* 3:575–84
25. Choi JH, Moon SH. 2001. Pore size characterization of cation-exchange membranes by chronopotentiometry using homologous amine ions. *J. Membr. Sci.* 191:225–36
26. Vlassiouk I, Smirnov S, Siwy Z. 2008. Ionic selectivity of single nanochannels. *Nano Lett.* 8:1978–85
27. Vlassiouk I, Apel PY, Dmitriev SN, Healy K, Siwy ZS. 2009. Versatile ultrathin nanoporous silicon nitride membranes. *Proc. Natl. Acad. Sci. USA* 106:21039–44
28. Yossifon G, Chang HC. 2008. Selection of nonequilibrium overlimiting currents: universal depletion layer formation dynamics and vortex instability. *Phys. Rev. Lett.* 101:254501
29. Yossifon G, Mushenheim P, Chang YC, Chang HC. 2009. Nonlinear current-voltage characteristics of nanochannels. *Phys. Rev. E* 79:046305
30. Duan CH, Majumdar A. 2010. Anomalous ion transport in 2-nm hydrophilic nanochannels. *Nat. Nanotechnol.* 5:848–52
31. Bottenus D, Oh YJ, Han SM, Ivory CF. 2009. Experimentally and theoretically observed native pH shifts in a nanochannel array. *Lab Chip* 9:219–31
32. Svoboda M, Slouka Z, Schrott W, Snita D. 2009. Cation exchange membrane integrated into a microfluidic device. *Microelectron. Eng.* 86:1371–74
33. Slouka Z, Senapati S, Yan Y, Chang HC. 2013. Charge inversion, water splitting, and vortex suppression due to DNA sorption on ion-selective membranes and their ion-current signatures. *Langmuir* 29:8275–83

34. Svoboda M, Kratochvila J, Lindner J, Pribyl M, Snita D. 2011. Dynamic behaviour of a diffusion layer around a cation-exchange membrane in an external electric field. *Microelectron. Eng.* 88:1789–91
35. Kwak R, Guan GF, Peng WK, Han JY. 2013. Microscale electrodialysis: concentration profiling and vortex visualization. *Desalination* 308:138–46
36. Cheng LJ, Chang HC. 2011. Microscale pH regulation by splitting water. *Biomicrofluidics* 5:046502
37. Ko SH, Song YA, Kim SJ, Kim M, Han J, Kang KH. 2012. Nanofluidic preconcentration device in a straight microchannel using ion concentration polarization. *Lab Chip* 12:4472–82
38. Frilette VJ. 1957. Electrogravitational transport at synthetic ion exchange membrane surfaces. *J. Phys. Chem. B* 61:168–74
39. Krol JJ, Wessling M, Strathmann H. 1999. Concentration polarization with monopolar ion exchange membranes: current-voltage curves and water dissociation. *J. Membr. Sci.* 162:145–54
40. Belova E, Lopatkova G, Pismenskaya N, Nikonenko V, Larchet C. 2006. Role of water splitting in development in ion-exchange membrane of electroconvection systems. *Desalination* 199:59–61
41. Belova EI, Lopatkova GY, Pismenskaya ND, Nikonenko VV, Larchet C, Pourcelly G. 2006. Effect of anion-exchange membrane surface properties on mechanisms of overlimiting mass transfer. *J. Phys. Chem. B* 110:13458–69
42. Choi JH, Kim SH, Moon SH. 2001. Heterogeneity of ion-exchange membranes: the effects of membrane heterogeneity on transport properties. *J. Colloid Interface Sci.* 241:120–26
43. Rubinstein I, Staude E, Kedem O. 1988. Role of the membrane-surface in concentration polarization at ion-exchange membrane. *Desalination* 69:101–14
44. Andersen MB, van Soestbergen M, Mani A, Bruus H, Biesheuvel PM, Bazant MZ. 2012. Current-induced membrane discharge. *Phys. Rev. Lett.* 109:108301
45. Maletzki F, Rosler HW, Staude E. 1992. Ion transfer across electrodialysis membranes in the overlimiting current range: stationary voltage current characteristics and current noise power spectra under different conditions of free convection. *J. Membr. Sci.* 71:105–15
46. Rubinstein I, Maletzki F. 1991. Electroconvection at an electrically inhomogeneous permselective membrane surface. *J. Chem. Soc.-Faraday Trans.* 87:2079–87
47. Rubinstein I, Zaltzman B. 2000. Electro-osmotically induced convection at a permselective membrane. *Phys. Rev. E* 62:2238–51
48. Druzgalski CL, Andersen MB, Mani A. 2013. Direct numerical simulation of electroconvective instability and hydrodynamic chaos near an ion-selective surface. *Phys. Fluids* 25:110804–17
49. Pham VS, Li ZR, Lim KM, White JK, Han JY. 2012. Direct numerical simulation of electroconvective instability and hysteretic current-voltage response of a permselective membrane. *Phys. Rev. E* 86:046310
50. Nandigana VVR, Aluru NR. 2012. Understanding anomalous current-voltage characteristics in microchannel-nanochannel interconnect devices. *J. Colloid Interface Sci.* 384:162–71
51. Yossifon G, Mushenheim P, Chang HC. 2010. Controlling nanoslot overlimiting current with the depth of a connecting microchamber. *EPL* 90:64004
52. Yossifon G, Chang HC. 2010. Changing nanoslot ion flux with a dynamic nanocolloid ion-selective filter: secondary overlimiting currents due to nanocolloid-nanoslot interaction. *Phys. Rev. E* 81:066317
53. Yossifon G, Mushenheim P, Chang YC, Chang HC. 2010. Eliminating the limiting-current phenomenon by geometric field focusing into nanopores and nanoslots. *Phys. Rev. E* 81:046301
54. Cheng LJ, Guo LJ. 2010. Entrance effect on ion transport in nanochannels. *Microfluid Nanofluid* 9:1033–39
55. Wang YC, Stevens AL, Han JY. 2005. Million-fold preconcentration of proteins and peptides by nanofluidic filter. *Anal. Chem.* 77:4293–99
56. Li GB, Wang SL, Byun CK, Wang XY, Liu SR. 2009. A quantitative model to evaluate the ion-enrichment and ion-depletion effect at microchannel-nanochannel junctions. *Anal. Chim. Acta* 650:214–20
57. Wang Y, Pant K, Chen ZJ, Wang GR, Diffey WF, et al. 2009. Numerical analysis of electrokinetic transport in micro-nanofluidic interconnect preconcentrator in hydrodynamic flow. *Microfluid Nanofluid* 7:683–96
58. Kim SJ, Ko SH, Kwak R, Posner JD, Kang KH, Han J. 2012. Multi-vortical flow inducing electrokinetic instability in ion concentration polarization layer. *Nanoscale* 4:7406–10

59. Ehlert S, Hlushkou D, Tallarek U. 2008. Electrohydrodynamics around single ion-permselective glass beads fixed in a microfluidic device. *Microfluid Nanofluid* 4:471–87
60. Ben Y, Chang HC. 2002. Nonlinear Smoluchowski slip velocity and micro-vortex generation. *J. Fluid Mech.* 461:229–38
61. Chang HC, Yossifon G, Demekhin EA. 2012. Nanoscale electrokinetics and microvortices: how microhydrodynamics affects nanofluidic ion flux. *Annu. Rev. Fluid Mech.* 44:401–26
62. Harnisch F, Schroder U, Scholz F. 2008. The suitability of monopolar and bipolar ion exchange membranes as separators for biological fuel cells. *Environ. Sci. Technol.* 42:1740–46
63. Aritomi T, van den Boomgaard T, Strathmann H. 1996. Current-voltage curve of a bipolar membrane at high current density. *Desalination* 104:13–18
64. Conroy DT, Craster RV, Matar OK, Cheng LJ, Chang HC. 2012. Nonequilibrium hysteresis and Wien effect water dissociation at a bipolar membrane. *Phys. Rev. E* 86:056104
65. Desharnais BM, Lewis BAG. 2002. Electrochemical water splitting at bipolar interfaces of ion exchange membranes and soils. *Soil Sci. Soc. Am. J.* 66:1518–25
66. Wang XY, Cheng C, Wang SL, Liu SR. 2009. Electroosmotic pumps and their applications in microfluidic systems. *Microfluid Nanofluid* 6:145–62
67. Paul PH, Arnold DW, Rakestraw DJ. 2000. Electrokinetic generation of high pressures using porous microstructures. *Micro Total Anal. Syst.* 1998:49–52
68. Zeng SL, Chen CH, Mikkelsen JC, Santiago JG. 2001. Fabrication and characterization of electroosmotic micropumps. *Sens. Actuators B* 79:107–14
69. Zeng SL, Chen CH, Santiago JG, Chen JR, Zare RN, et al. 2002. Electroosmotic flow pumps with polymer frits. *Sens. Actuators B* 82:209–12
70. Tripp JA, Svec F, Frechet JMJ, Zeng SL, Mikkelsen JC, Santiago JG. 2004. High-pressure electroosmotic pumps based on porous polymer monoliths. *Sens. Actuators B* 99:66–73
71. Wang P, Chen ZL, Chang HC. 2006. A new electro-osmotic pump based on silica monoliths. *Sens. Actuators B* 113:500–9
72. Berrouche Y, Avenas Y, Schaeffer C, Chang HC, Wang P. 2009. Design of a porous electroosmotic pump used in power electronic cooling. *IEEE Trans. Ind. Appl.* 45:2073–79
73. Chen Z, Wang P, Chang HC. 2005. An electro-osmotic micro-pump based on monolithic silica for micro-flow analyses and electro-sprays. *Anal. Bioanal. Chem.* 382:817–24
74. Wang SC, Wei HH, Chen HP, Tsai MH, Yu CC, Chang HC. 2008. Dynamic superconcentration at critical-point double-layer gates of conducting nanoporous granules due to asymmetric tangential fluxes. *Biomicrofluidics* 2:014102
75. Cheng LJ, Guo LJ. 2010. Nanofluidic diodes. *Chem. Soc. Rev.* 39:923–38
76. Nguyen G, Vlassiouk I, Siwy ZS. 2010. Comparison of bipolar and unipolar ionic diodes. *Nanotechnology* 21:265301
77. Yossifon G, Chang YC, Chang HC. 2009. Rectification, gating voltage, and interchannel communication of nanoslot arrays due to asymmetric entrance space charge polarization. *Phys. Rev. Lett.* 103:154502
78. Jung JY, Joshi P, Petrossian L, Thornton TJ, Posner JD. 2009. Electromigration current rectification in a cylindrical nanopore due to asymmetric concentration polarization. *Anal. Chem.* 81:3128–33
79. Cheng LJ, Guo LJ. 2007. Rectified ion transport through concentration gradient in homogeneous silica nanochannels. *Nano Lett.* 7:3165–71
80. Garcia-Gimenez E, Alcaraz A, Aguilella VM, Ramirez P. 2009. Directional ion selectivity in a biological nanopore with bipolar structure. *J. Membr. Sci.* 331:137–42
81. Apel PY, Blonskaya IV, Levkovich NV, Orelovich OL. 2011. Asymmetric track membranes: relationship between nanopore geometry and ionic conductivity. *Pet. Chem.* 51:555–67
82. Hlushkou D, Perry JM, Jacobson SC, Tallarek U. 2012. Propagating concentration polarization and ionic current rectification in a nanochannel-nanofunnel device. *Anal. Chem.* 84:267–74
83. Perry JM, Zhou KM, Harms ZD, Jacobson SC. 2010. Ion transport in nanofluidic funnels. *ACS Nano* 4:3897–902
84. Yan RX, Liang WJ, Fan R, Yang PD. 2009. Nanofluidic diodes based on nanotube heterojunctions. *Nano Lett.* 9:3820–25

85. Karnik R, Duan CH, Castelino K, Daiguji H, Majumdar A. 2007. Rectification of ionic current in a nanofluidic diode. *Nano Lett.* 7:547–51
86. Constantin D, Siwy ZS. 2007. Poisson-Nernst-Planck model of ion current rectification through a nanofluidic diode. *Phys. Rev. E* 76:041202
87. Vlassiouk I, Siwy ZS. 2007. Nanofluidic diode. *Nano Lett.* 7:552–56
88. Miedema H, Vrouenraets M, Wierenga J, Meijberg W, Robillard G, Eisenberg B. 2007. A biological porin engineered into a molecular, nanofluidic diode. *Nano Lett.* 7:2886–91
89. Venkatesan BM, Bashir R. 2011. Nanopore sensors for nucleic acid analysis. *Nat. Nanotechnol.* 6:615–24
90. Liu AH, Zhao QT, Guan XY. 2010. Stochastic nanopore sensors for the detection of terrorist agents: current status and challenges. *Anal. Chim. Acta* 675:106–15
91. Jayawardhana DA, Crank JA, Zhao Q, Armstrong DW, Guan XY. 2009. Nanopore stochastic detection of a liquid explosive component and sensitizers using boromycin and an ionic liquid supporting electrolyte. *Anal. Chem.* 81:460–64
92. Krishantha DMM, Breitbach ZS, Padivitage NLT, Armstrong DW, Guan XY. 2011. Rapid determination of sample purity and composition by nanopore stochastic sensing. *Nanoscale* 3:4593–96
93. Lee JH, Song YA, Han JY. 2008. Multiplexed proteomic sample preconcentration device using surface-patterned ion-selective membrane. *Lab Chip* 8:596–601
94. Liu V, Song YA, Han JY. 2010. Capillary-valve-based fabrication of ion-selective membrane junction for electrokinetic sample preconcentration in PDMS chip. *Lab Chip* 10:1485–90